AIAA JOURNAL
Vol. 34, No. 10, October 1996

Implementation of an Adaptive Piezoelectric Sensoriactuator

Jeffrey S. Vipperman* and Robert L. Clark†
Duke University, Durham, North Carolina 27708-0302

An adaptive algorithm implemented on a digital signal processor is used in conjunction with an analog multiplier circuit to compensate for the feedthrough capacitance of a piezoelectric sensoriactuator. The mechanical response of the piezoelectric sensoriactuator is resolved from the electrical response by adaptively altering the gain imposed on the electrical circuit used for compensation. For broadband, stochastic input disturbances, the feedthrough dynamic capacitance of the sensoriactuator can be identified on-line, providing a means of implementing direct-rate-feedback control in analog hardware. Rate feedback control is demonstrated on a cantilevered beam using the hybrid/adaptive circuit. The ability of the circuit to readapt to a change in capacitance is demonstrated by a simple experiment.

Nomenclature

C	= capacitor, capacitance
$\boldsymbol{C}_p$	= capacitance matrix of piezoceramic
$\mathcal{D}$	= damping matrix
$E[\cdot]$	= expectation operator
f_c	= cutoff frequency
$h(n)$	= unit sample response
i	= current
k	= discrete time step
$\mathcal{L}[\cdot]$	= Laplacian transform operator
$\boldsymbol{q}$	= charge on piezoelectric patch
R	= resistor
$\boldsymbol{r}$	= modal displacement
$\ddot{\boldsymbol{r}}$	= modal acceleration
s	= Laplacian variable
t	= time
V, v	= volts, voltage
w	= digital filter weight
∂	= partial differential operator
$\delta(n)$	= Dirac delta function
Θ	= electromechanical coupling matrix of piezoceramic
μ	= convergence parameter
$\phi_{xy}(n)$	= discrete correlation function between $x(n)$ and $y(n)$
Ω^2	= matrix of natural frequencies
∇	= gradient operator

Subscripts

DSP	= digital signal processor
elec	= electrical
mech	= mechanical
Out	= output signal
p	= piezoceramic
pa	= power amplifier
R	= reference leg
01	= leg 1 of conditioning circuit
02	= leg 2 of conditioning circuit
03	= leg 3 of conditioning circuit

Introduction

IN recent studies, Anderson et al.[1] and Dosch et al.[2] demonstrated the potential of using a piezoelectric transduction device simultaneously for sensing and actuation. Because of the stability associated with collocated transduction devices in direct-feedback-control loops, concurrent use of the same device as a sensor and an actuator has many applications in the aerospace industry. Piezoelectric transduction devices have been suggested for use in the suppression of flutter in panels,[3] platelike lifting surfaces,[4] and in airfoils.[5-7] The transduction devices also have been considered as elements of adaptive structures for active structural acoustic control,[8,9] for the suppression of interior noise within the fuselage of modern aircraft,[10-13] and for adding damping to flexible truss structures as required for large space structures.[14-20] In the present work, a method of adaptively compensating for the feedthrough dynamics associated with the electrical response of the sensoriactuator is demonstrated experimentally with hybrid analog and digital electronics.

The piezostructure, defined as the combination of the structure and its surface-mounted or embedded piezoelectric components, can be described by the second-order multiple-degree-of-freedom equation[21]

$$\text{Actuator: } \ddot{\boldsymbol{r}} + \mathcal{D}\dot{\boldsymbol{r}} + \Omega^2 \boldsymbol{r} = \Theta v \tag{1}$$

$$\text{Sensor: } \boldsymbol{q} = \Theta^T \boldsymbol{r} + \boldsymbol{C}_p v \tag{2}$$

Thus, if the capacitance of the piezoelectric device is known, one must simply apply the same voltage across an identical capacitor and subtract the electrical response from that of the sensoriactuator to resolve the mechanical response of the structure. A schematic diagram of an analog circuit used to resolve the mechanical strain rate from the electrical response is presented in Fig. 1. As illustrated, two current amplifiers are implemented such that the time derivative of charge (current) can be monitored.

As noted by Anderson et al.,[1] small errors in the identification of the capacitance of the sensoriactuator degrade the performance of the closed-loop control system. Because the electromechanical properties of the transduction device are subject to change in response to time-varying environmental and operating conditions, an alternative method of implementation is required. Cole and Clark[22] first proposed the use of adaptive signal processing to estimate the feedthrough capacitance of the piezoelectric device on-line. For a broadband, stochastic input, a single-coefficient adaptive filter can be used to compensate for the feedthrough capacitance of the piezostructure. Thus, the adaptive algorithm can be used to measure the dynamic capacitance of the device coupled to the structure for collocated feedback-control applications.

The work by Cole and Clark[22] is extended in this study for practical implementation of the sensoriactuator in hardware. Both analog and digital signal processing are used to achieve the sensoriactuator, and the capacitance of the device is estimated in situ for practical implementation of direct-rate feedback control. As discussed by Cole and Robertshaw,[23] as long as one underestimates the capacitance of the piezoelectric transduction device in the implementation of the sensoriactuator, the closed-loop control system is unconditionally

Received March 25, 1995; revision received Nov. 20, 1995; accepted for publication Dec. 29, 1995.

*Graduate Research Assistant, Department of Mechanical Engineering and Materials Science. Student Member AIAA.

†Assistant Professor, Department of Mechanical Engineering and Materials Science. Member AIAA.

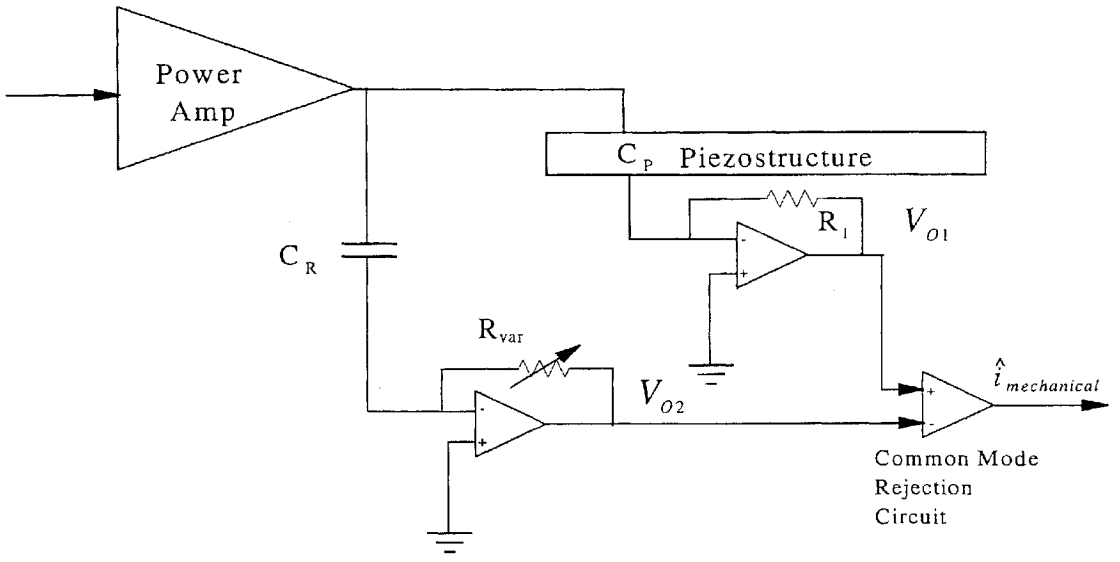

Fig. 1 Schematic diagram of passive analog compensation circuit.

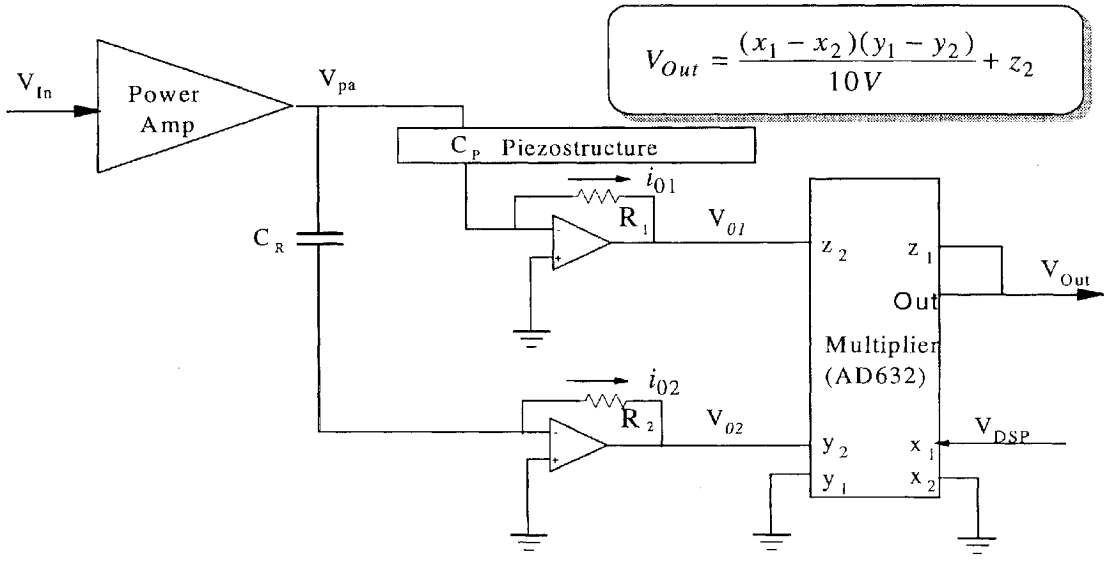

Fig. 2 Schematic diagram of hybrid analog/digital compensation circuit (sensoriactuator network).

stable (in the absence of amplifier dynamics). Results from this study demonstrate that adaptive compensation of piezoelectric sensoriactuators with analog and digital hardware offers a viable method for practical implementation.

Hybrid Analog and Digital Compensation

In past efforts, the primary hurdle in implementing a sensoriactuator has been in the accurate estimation of the capacitance of the piezoelectric device.[1,24] To circumvent this problem, the electrical circuit illustrated in Fig. 2 is proposed for adaptive compensation. The blending of the analog and digital circuitry is accomplished via the AD632 analog multiplier chip, which has a fairly linear response with a signal-to-noise ratio and common-mode rejection ratio of approximately 80 dB. By supplying a dc voltage (V_{DSP}) to one of the differential inputs and the signal to be scaled to the other differential input, a voltage-controlled amplifier (VCA) is achieved with the AD632. Further, the internal output of the VCA can be summed with input z_2 of the AD632, removing the need for a separate common-mode rejection circuit that differences the estimated electrical response from the total plant response (see Fig. 3). The dc voltage is controlled with a digital signal processor and is adapted with the least-mean-square (LMS) algorithm[25] as outlined previously by Cole and Clark.[22] The Appendix details the convergence of the adaptive filter and shows that the optimal Wiener filter solution is indeed the capacitance of the piezostructure. As indicated in Fig. 3, a third leg (V_{03}) can be added to differentiate the training signal that is used for adaptation so that any control signal would not potentially bias the filter solution during closed-loop operation.

After the adaptive filter has converged, the dynamic capacitance of the piezostructure has been matched. From Fig. 2,

$$V_{01}(s) = \mathcal{L}[-R_1 i_{01}(t)] \tag{3a}$$

$$= \mathcal{L}\left\{-R_1\left[C_p\frac{dv_{pa}(t)}{dt} + i_{mech}(t)\right]\right\} \tag{3b}$$

$$= -sR_1C_PV_{pa}(s) - R_1 i_{mech}(s) \tag{3c}$$

where all variables except $\mathcal{L}[\cdot]$, t, and s represent electronic components from the figure. Similarly,

$$V_{02}(s) = -sR_2C_RV_{pa}(s) \tag{4}$$

which leads to

$$V_{Out}(s) = \frac{V_{DSP}[-sR_2C_RV_{pa}(s)]}{10V} - sR_1C_PV_{pa}(s) - R_1 i_{mech}(s) \tag{5}$$

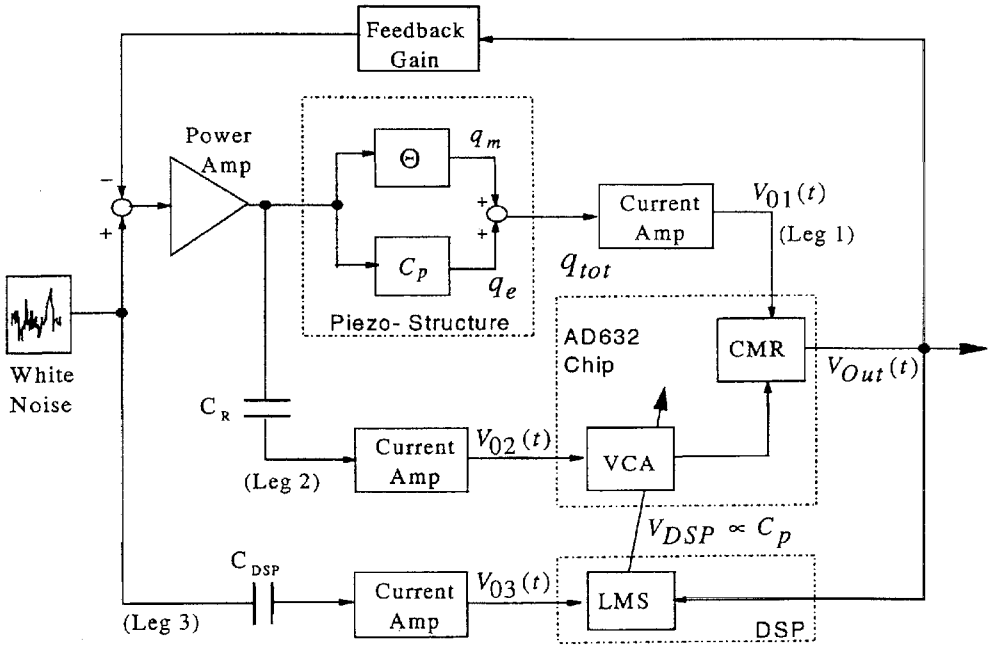

Fig. 3 Diagram of analog digital adaptive filter used to estimate the dynamic capacitance.

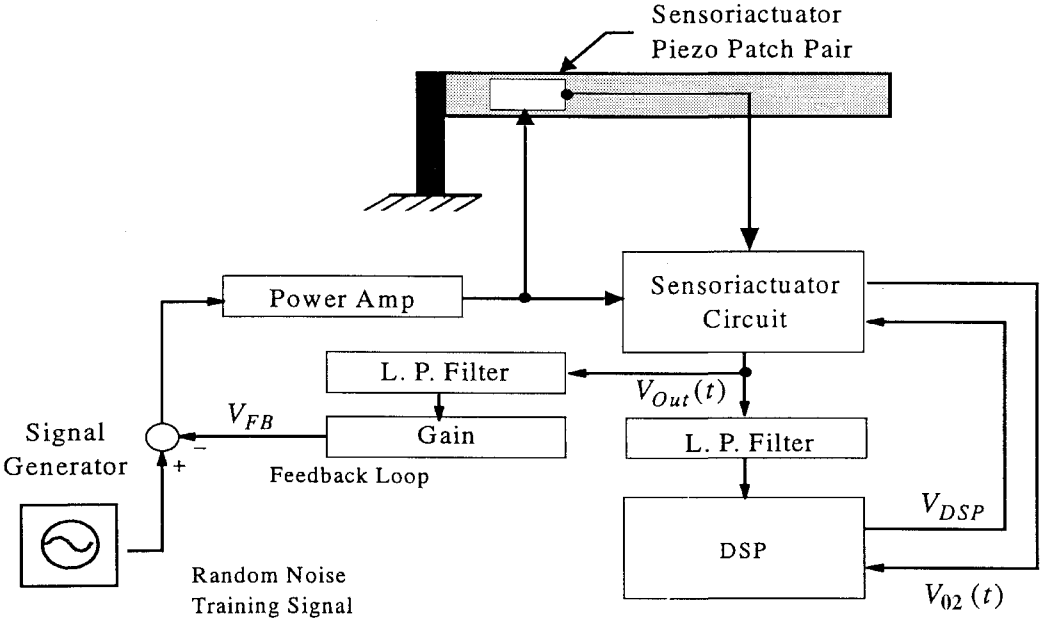

Fig. 4 Experimental setup.

where $10V$ is an internal gain for the AD632 multiplier chip. By inspection, for $V_{\text{Out}}(s)$ to equal only the mechanical response of the piezostructure $-R_1 i_{\text{mech}}$,

$$V_{\text{DSP}} \equiv \frac{10R_1C_P}{R_2C_R} \tag{6}$$

The quadratic cost function that is minimized by the LMS algorithm is defined as

$$C[w(k)] = E\left[V_{\text{Out}}^2\right] \tag{7}$$

where $w(k)$ is the digital filter weight. The quadratic cost is minimized using steepest descent

$$w(k+1) = w(k) - \mu\nabla C[w(k)] \tag{8a}$$

$$= w(k) - \mu 2E\left(V_{\text{Out}}\frac{\partial V_{\text{Out}}}{\partial w}\right) \tag{8b}$$

where μ is a step-size parameter that controls stability and convergence and $w(k)$ is the single-coefficient FIR filter required to adapt the capacitance, which is equivalent to the output voltage, V_{DSP}. The LMS algorithm uses a stochastic estimate of the gradient:

$$w(k+1) \approx w(k) + \mu 2V_{\text{Out}}(k)\frac{V_{02}(k)}{10V} \tag{9}$$

The difference here, is that the adaptive coefficient is implemented in analog $[V_{\text{DSP}} \equiv w(k+1)]$ such that the controller can be implemented in analog as well maintain stability guarantees associated with collocated rate-feedback control.[26]

Experimental Setup

The new sensoriactuator-based hybrid controller was demonstrated experimentally on a cantilevered beam. Figure 4 depicts the experimental setup. The beam was made of plain carbon steel and was clamped to an optical bench for the duration of the experiments.

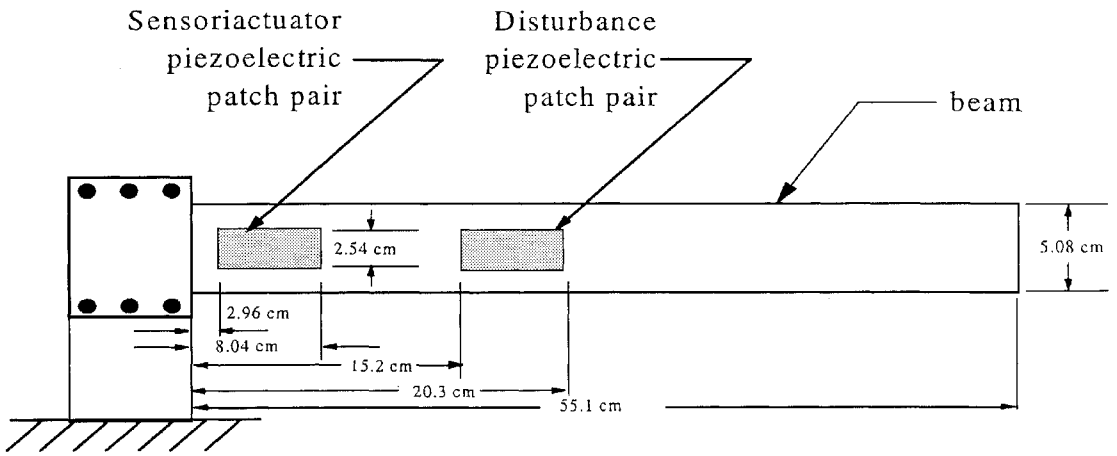

Fig. 5 Dimensions and locations of beam transducers.

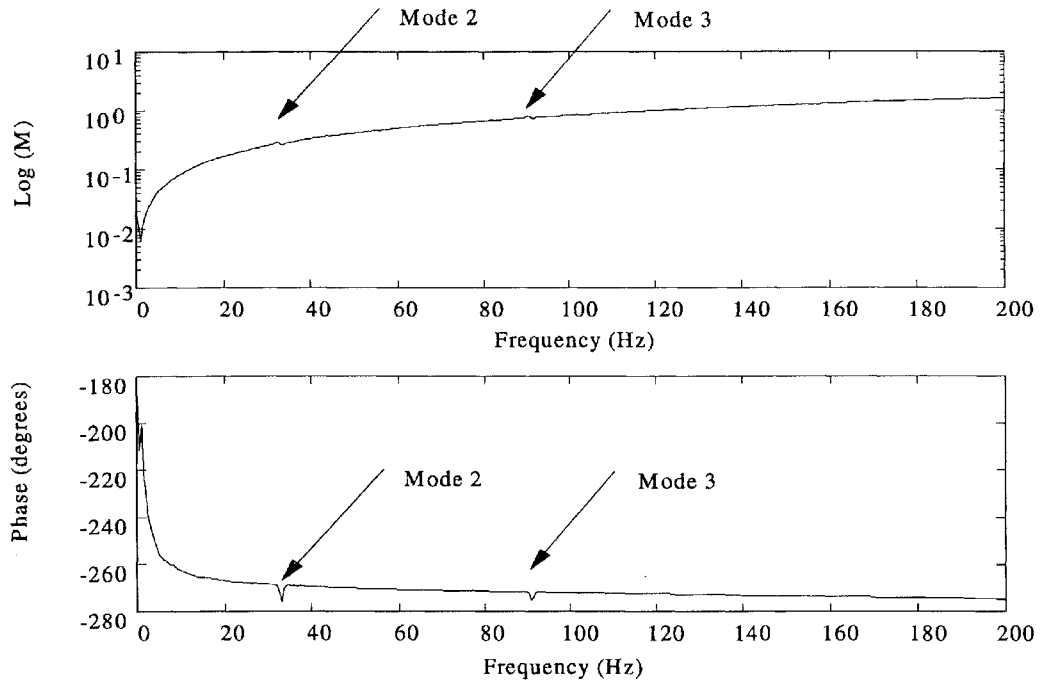

Fig. 6 Frequency response function of the uncompensated sensoriactuator.

Table 1 lists the theoretical and experimentally measured natural frequencies and damping ratios of the first four bending modes of the beam. These properties were estimated from the measured frequency response function (FRF) using a curve-fitting program. The sensoriactuator consisted of a piezoelectric bending motor coupled with the digital/analog circuit depicted in Fig. 2. The bending motor is a collocated set of lead zirconate titanate piezoceramic (PZT5A) patches mounted symmetrically about the beam surface and wired out of phase to produce pure bending (in theory) about the beam neutral axis. A second piezoelectric-patch pair located farther from the root of the beam was used as a disturbance source. The exact locations of these transducers as well as the beam dimensions are shown in Fig. 5.

A Krohn–Hite Model 7600 wideband amplifier was used to drive the sensoriactuator, and an Ithaco 4302 low-pass Bessel filter was used as an antialiasing filter before the sensoriactuator output was sampled with the digital signal processor (DSP) board. Another 4302 low-pass filter (f_c = 160 Hz) was used in the feedback loop to roll off the high-frequency response of the structure. A Tektronix 2630 four-channel spectrum analyzer was used for all time- and frequency-domain analysis, and an on-board signal generator was used to produce the broadband signal required to excite the sensoriactuator. The harmonic disturbance signal was supplied with a Wavetek 75A arbitrary waveform generator. A TMS320C30-based DSP in a pentium host computer was used for the adaptation of the analog circuit. The 16-bit analog I/O has a dynamic range of 101 dB when full scale is used. Dynamic range was maximized by using a simple gain circuit before the inputs to the analog I/O, when needed.

Table 1 Modal properties of beam

Mode	Theor. natural frequency, Hz	Measured resonant frequency, Hz	Measured damping ratio
1	5.39	5.27	0.00230
2	33.7	32.9	0.00950
3	94.2	91.1	0.00205
4	185	171	0.00750

Experimental Results

The open-loop response of the sensoriactuator was investigated experimentally. First, the circuit output with no compensation of the feedthrough dynamics (V_{DSP} = 0) was measured. The FRF between

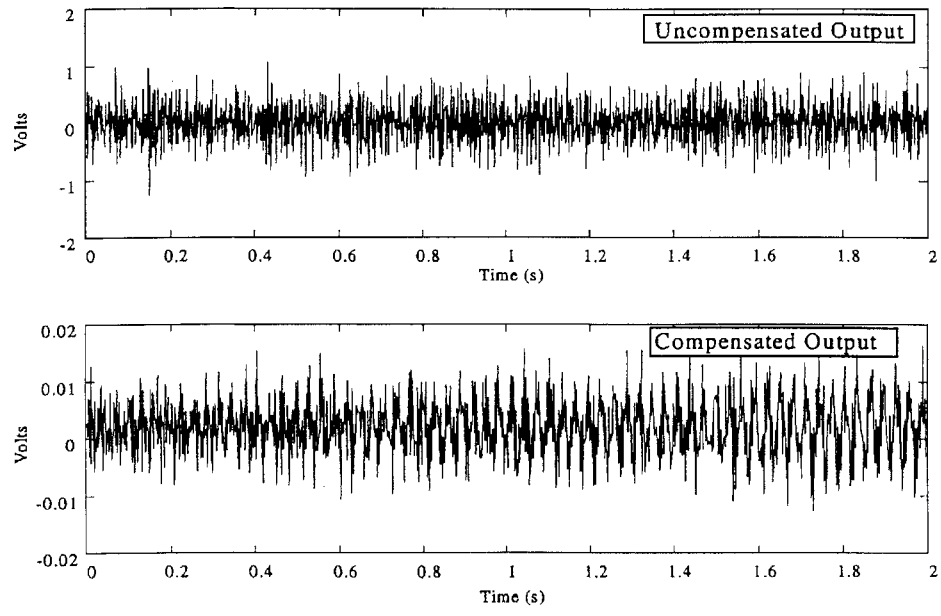

Fig. 7 Measured sensoriactuator output with and without analog/digital compensation.

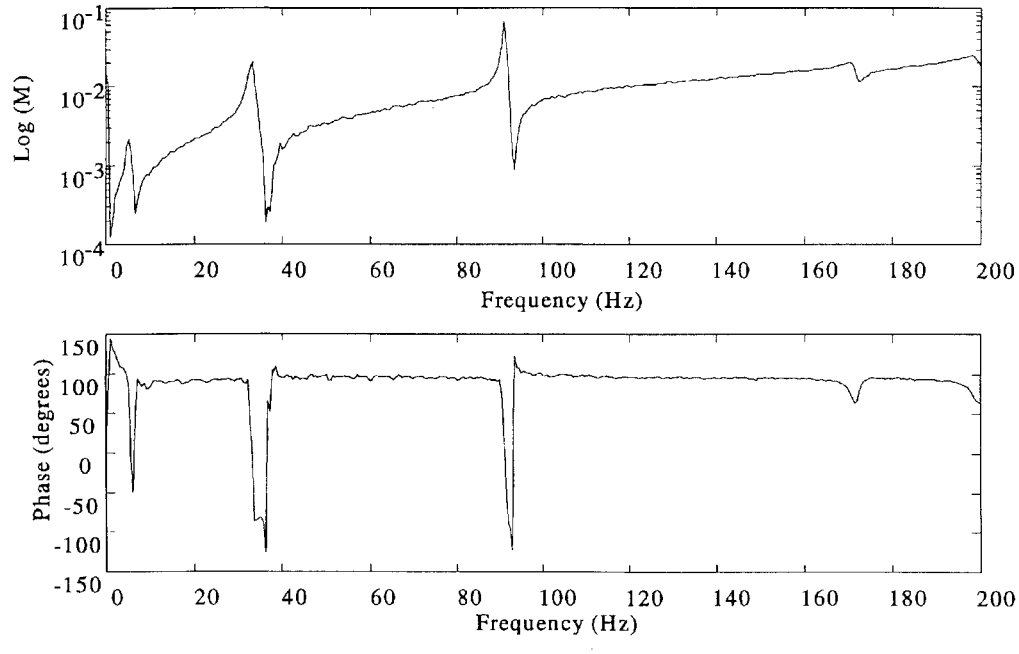

Fig. 8 Experimental frequency response of sensoriactuator with analog/digital compensation.

the 0- to 200-Hz random input and the sensoriactuator output signal is shown in Fig. 6. The curves generally reflect the high-pass characteristics of the capacitive electrical response of the piezoelectric element and the free-field wave propagating on the beam. The resonant peaks of the second and third beam modes can barely be recognized, as denoted in Fig. 6. It is evident from Fig. 6 that the signal resulting from the electrical response dominates the total signal when no electrical compensation is present. Next, the digital-feedthrough-compensation filter was allowed to adapt by setting the convergence parameter to 0.05 and the sampling rate of the DSP to 2 kHz. A much smaller signal results because the current induced in the piezoceramic transducer by the applied voltage is much larger than that induced in the device by the mechanical strain. Figure 7 shows the voltage signals measured from the sensoriactuator circuit, with and without feedthrough compensation. The compensated output is roughly two orders of magnitude smaller than the uncompensated signal, bringing to light the difficulty associated with extracting the mechanical response (a dynamic-range issue). Tuning the circuit by hand, with a variable-gain current amplifier (Fig. 1) is normally a tedious process. As indicated in Fig. 2, a reference capacitor is used for gross phase-compensation for the piezoceramic and also ensures that the maximum dynamic range of the DSP can be utilized in the fine-tuning process. Computing the FRF of the compensated output reveals the dynamics of the beam (Fig. 8). The frequency response of the analytical model having no capacitive feedthrough dynamics is shown in Fig. 9 and good agreement with the experimental FRF is observed. The discrepancy in the scaling is simply a result of analog gains required in the actual experimental implementation.

Closed-Loop Control

Control of the beam response was demonstrated while simultaneously adapting the capacitance of the piezoelectric patch. A low-level band-limited random noise was used to provide the training

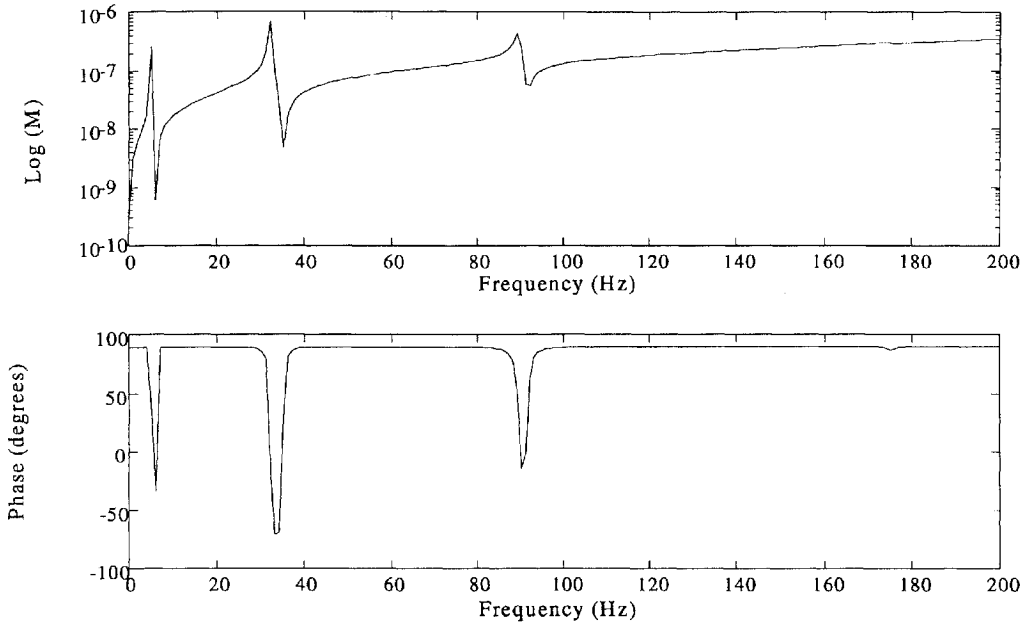

Fig. 9 Analytical frequency response of sensoriactuator with no feedthrough dynamics.

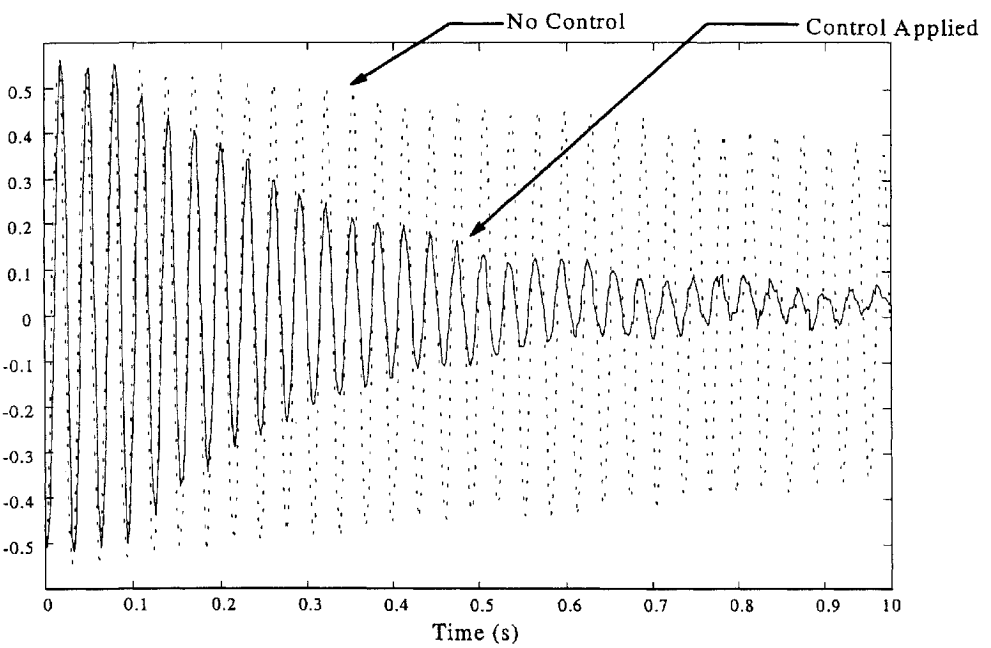

Fig. 10 Application of RFB control using the hybrid adaptive sensoriactuator.

signal for the adaptive sensoriactuator while having a relatively insignificant effect on the system response. The adaptive digital filter can only remove components of the sensoriactuator circuit output that are coherent to the input of the adaptive digital filter, i.e., $V_{02}(t)$, whereas all other signals will not affect the adaptation process. Hence, it is possible to adapt the sensoriactuator while using it for control of persistent or transient disturbances.

To demonstrate control, the beam was driven near the second-mode resonance and allowed to freely decay. The same experiment was repeated with the rate-feedback control applied. The locations of the poles and zeros along with the limited bandwidth of the controller made the second mode the best candidate for active damping for this particular system. Figure 10 shows this free response of the beam with and without rate feedback (RFB) control overlaid with each other. The magnitudes of the time histories have been adjusted by a factor of 2.7 so that steady-state values of the time histories are equivalent because RFB control significantly increases the plant impedance at resonance. A log decrement calculation was used to estimate the increase in damping: more than a factor of six when RFB control is applied. After the disturbance is removed and the beam response decays to steady state, one can vaguely see the random noise that is used to tune the sensoriactuator circuit. The output voltage V_{DSP} was monitored and remained relatively constant during the process and consequently is not shown here.

Dynamic Calculation of Patch Capacitance

An important result of this work is the ability to dynamically measure the pseudoblocked capacitance in situ. The term pseudoblocked was chosen because the structure has some compliance. By knowing the internal gains across the sensoriactuator network and the

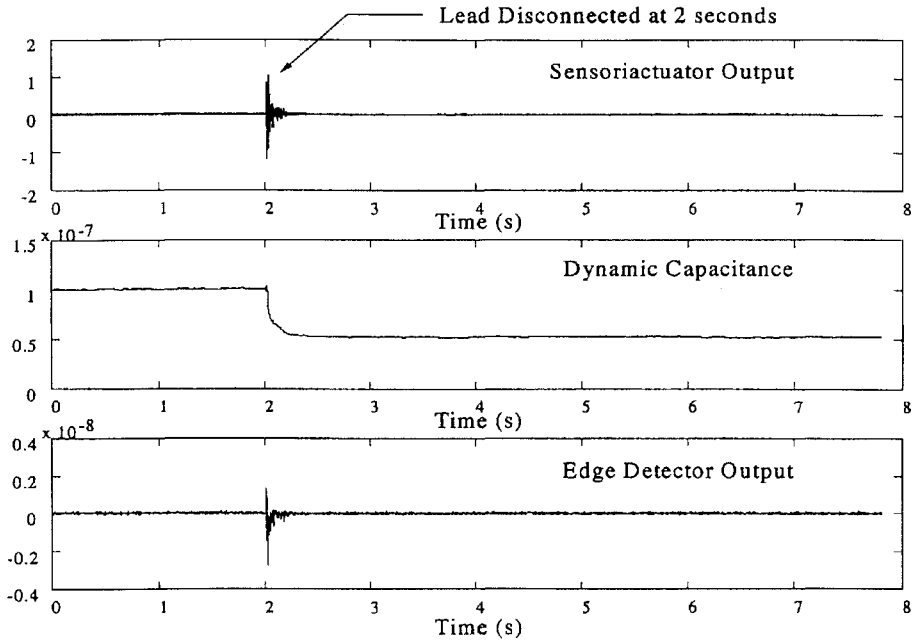

Fig. 11 Readaptation of the capacitance after one of the piezoelectric patches in the bending motor is disconnected.

reference capacitance, the pseudoblocked capacitance for this sensoriactuator is

$$C_P^s = \frac{R_2 V_{\mathrm{DSP}}}{(10V)R_1} C_R \tag{10a}$$

$$= \frac{(4.31k\Omega)(5.29V)}{(2.192k\Omega)(10V)} 0.104\,\mu\mathrm{F} = 0.108\,\mu\mathrm{F} \tag{10b}$$

where R_1 and R_2 are gain resistors depicted in Fig. 2 and C_R is the reference capacitor. When the capacitance of the mounted piezo bending motor is measured using a Fluke 87 multimeter, a value of 0.112 μF is observed. Therefore, an error of 3.7% in the estimation of the capacitance would have resulted. This overestimation of the blocked capacitance can potentially lead to instabilities in rate feedback control.[1,19,23] The Fluke meter charges the piezoceramic element to measure capacitance, imparting a strain upon the ceramic, where in contrast, the in situ method presented here measures the capacitance using a zero-mean process. Slight changes in the measured and estimated capacitances have been observed, resulting from minor fluctuations in the laboratory environment. Again, the adaptive sensoriactuator can easily track and compensate for any changes in the operating capacitance.

Readaptation After a Capacitance Change

The ability of the algorithm to readapt to a change in the operating capacitance is demonstrated by a simple experiment in which one of the two patches that make up the sensoriactuator bending motor is suddenly disconnected. In the topmost time history of Fig. 11, it can be seen that the output of the sensoriactuator was dominated briefly by the electrical response shortly after the second patch was removed from the circuit. The circuit readapts and, as expected, the capacitance is now half of the original value (middle time history of Fig. 11). Last, in the bottom frame, the potential of using the adaptive sensoriactuator for on-line system health monitoring is demonstrated. A spike is seen in the output of an edge detector (discrete differentiator),[27] indicating that a change in capacitance has occurred. The output of the edge detector, $y(k)$ is the difference between the present and the past estimated discrete dynamic capacitance values (no new signals need to be sampled), $\hat{C}_p(k)$, $\hat{C}_p(k-1)$:

$$y(k) = \hat{C}_p(k) - \hat{C}_p(k-1) \tag{11}$$

where k is the sample index. Decimation[27] could be used to monitor the capacitance across many different timescales.[28]

Conclusions

The use of a single piezoelectric element for simultaneous sensing and actuation of mechanical structures has many applications in the aerospace industry, including flutter suppression, control of structure-borne sound in the fuselage of aircraft, and control of large space structures. An alternative method of compensating for the electrical feedthrough dynamics associated with the capacitance of piezoceramic sensoriactuators based upon adaptive signal processing and a combination of analog and digital hardware is demonstrated.

The method presented herein provides a technique for adaptive compensation of the sensoriactuator on-line: producing a more accurate estimate of the blocked capacitance, and providing a method of monitoring changes that occur in the transduction device during operation. Results from this work indicate that a dynamic estimation of the blocked capacitance of the device in situ results in a lower value than that measured under static conditions (3.7% for the case presented). The measured frequency response of a cantilevered beam configured with a sensoriactuator compared well with the predicted frequency response of the same computed from an analytical model. Experimental work using a sensoriactuator attached to a clamped-free steel beam demonstrated the operation of the adaptive sensoriactuator for rate-feedback-control applications. One simple experiment demonstrated the ability of the circuit to retune itself if the piezoelectric transducer is altered or damaged in some way.

Future work will address nonideal behavior (e.g., nonlinearities, complex behavior of the dielectric constant) in piezoceramic transducers.

Appendix A: Convergence of the LMS Filter

The convergence of the LMS algorithm to the capacitance of the piezostructure is presented, as adapted from work by Cole and Clark.[22] It is well established that the LMS algorithm converges in the mean to the optimal Wiener filter solution for stationary input signals.[25] The optimal Wiener filter solution is expressed as

$$W_{\mathrm{opt}} = \boldsymbol{R}^{-1}\boldsymbol{p} \tag{A1}$$

where W_{opt} is the Wiener solution, $\boldsymbol{R}$ is the input correlation matrix for the adaptive filter, $\boldsymbol{p}$ is the cross-correlation vector between the input to the filter and the desired signal plus noise, which from Fig. 2 is

$$\boldsymbol{R} = E[V_{02}(n)V_{02}(n)] = \phi_{V_{02}V_{02}}(n) \tag{A2a}$$

$$\boldsymbol{p} = E[V_{02}(n)V_{01}(n)] = \phi_{V_{01}V_{02}}(n) \tag{A2b}$$

where n is the sample index, and $\phi_{V_{01}V_{01}}(n)$, $\phi_{V_{02}V_{02}}(n)$, $\phi_{V_{01}V_{02}}(n)$ are the discrete auto- or cross-correlation functions between signals V_{01} and V_{02}. Substituting Eqs. (A2a) and (A2b) into Eq. (A1) yields

$$W_{\text{opt}} = \frac{\phi_{V_{01}V_{02}}}{\phi_{V_{02}V_{02}}} \tag{A3}$$

We can further express the signals that make up the correlation functions in Eq. (A3) in terms of the electrical components from Figs. 2 and 3 and the discrete structural impulse response $h(i)$ as

$$V_{01}(n) = R_1 C_p \frac{\mathrm{d}}{\mathrm{d}t} V_{\text{pa}}(n) + R_1 \frac{\mathrm{d}}{\mathrm{d}t} q_{\text{mech}}(n) \tag{A4a}$$

$$= R_1 C_p \dot{V}_{\text{pa}}(n) + R_1 \sum_{i=0}^{\infty} h(i) \dot{V}_{\text{pa}}(n-i) \tag{A4b}$$

$$V_{02}(n) = \frac{R_2 C_R \dot{V}_{\text{pa}}(n)}{10V} \tag{A4c}$$

Substituting Eqs. (A4b) and (A4c) into Eq. (A3) and simplifying yields

$$W_{\text{opt}} = \frac{R_1 10V}{R_2 C_r} C_p + \frac{R_1 10V \sum_{i=0}^{\infty} h(i) \phi_{\dot{V}_{\text{pa}}\dot{V}_{\text{pa}}}(n-i)}{R_2 C_R \phi_{\dot{V}_{\text{pa}}\dot{V}_{\text{pa}}}(n)} \tag{A5}$$

One can take advantage of the fact that $h(0) = 0$ for a causal system by using a training signal in which each sample value is uncorrelated with all other samples [i.e., random noise: $\phi_{V_{\text{pa}}V_{\text{pa}}}(n) = \sigma_{\text{pa}}^2 \delta(n)$]. In this case, the optimal Wiener solution becomes

$$W_{\text{opt}} = \frac{R_1 10V}{R_2 C_R} C_p \tag{A6}$$

which is consistent with Eq. (6).

Acknowledgment

The authors gratefully acknowledge the Structural Acoustics Branch at NASA Langley Research Center for funding this research under Grant NAG-1-1570.

References

[1]Anderson, E. H., Hagood, N. W., and Goodliffe, J. M., "Self-Sensing Piezoelectric Actuation: Analysis and Application to Controlled Structures," *Proceedings of the AIAA/ASME/ASCE/AHS/ASC 33rd Structures, Structural Dynamics, and Materials Conference* (Dallas, TX), AIAA, Washington, DC, 1992, pp. 2141–2155.

[2]Dosch, J. J., Inman, D. J., and Garcia, E., "A Self-Sensing Piezoelectric Actuator for Colocated Control," *Journal of Intelligent Material Systems and Structures*, Vol. 3, Jan. 1992, pp. 166–185.

[3]Frampton, K. D., and Clark, R. L., Jr., "Active Control of Panel Flutter with Linearized Potential Flow," *Proceedings of the AIAA/ASME/ASCE/AHS/ASC 36th Structures, Structural Dynamics, and Materials Conference* (New Orleans, LA), AIAA, Washington, DC, 1995, pp. 2273–2280.

[4]Lazarus, K. B., and Crawley, E. F., "Multivariable High-Authority Control of Plate-Like Active Structures," *Proceedings of the AIAA/ASME/ASCE/AHS/ASC 33rd Structures, Structural Dynamics, and Materials Conference* (Dallas, TX), AIAA, Washington, DC, 1992, pp. 931–945.

[5]Lazarus, K. B., Crawley, E. F., and Bohlmann, J. D., "Static Aeroelastic Control Using Strain Actuated Adaptive Structures," *Journal of Intelligent Material Systems and Structures*, Vol. 2, No. 3, 1991, pp. 386–440.

[6]Lazarus, K. B., and Crawley, E. F., "Multivariable Active Lifting Surface Control Using Strain Actuation: Analytical and Experimental Results," *Proceedings of the 3rd International Conference on Adaptive Structures* (San Diego, CA), 1992, pp. 87–101.

[7]Saunders, W. R., Cole, D. G., Mook, D. T., Robertshaw, H. H., Monaco, J. F., and Ward, D. G., "Smart Structures for Active Control of Aircraft Systems," Adaptive Technologies, TR, ATI-95-002, Blacksburg, VA, 1995.

[8]Clark, R. L., and Fuller, C. R., "Control of Sound Radiation with Adaptive Structures," *Journal of Intelligent Material Systems and Structures*, Vol. 2, No. 3, 1991, pp. 431–452.

[9]Clark, R. L., and Fuller, C. R., "Experiments on Active Control of Structurally Radiated Sound Using Multiple Piezoceramic Actuators," *Journal of the Acoustical Society of America*, Vol. 91, No. 6, 1991, pp. 3313–3320.

[10]Fuller, C. R., Snyder, S., Hansen, C., and Silcox, R. J., "Active Control of Interior Noise in Model Aircraft Fuselages Using Piezoceramic Actuators," *AIAA Journal*, Vol. 30, No. 11, 1992, pp. 2613–2617.

[11]Cabell, R. H., Lester, H. C., Mathur, G. P., and Tran, B. N., "Optimization of Actuator Arrays for Aircraft Interior Noise Control," AIAA Paper 93-4447, Oct. 1993.

[12]Coats, T., Silcox R. J., and Lester H. C., "Numerical Study of Active Structural Acoustic Control in a Double-Walled Cylinder," *Proceedings of Recent Advances in Active Control of Sound and Vibration* (Blacksburg, VA), 1993.

[13]Silcox, R. J., Lyle, K. H., Metcalf, V. L., and Brown, D. E., "A Study of Active Structural Acoustic Control Applied to the Trim Panels of a Large Scale Fuselage Model," First Joint CEAS/AIAA Aeroacoustics Conf., Munich, Germany, June 1995.

[14]Forward, R. L., "Electronic Damping of Vibrations in Optical Structures," *Applied Optics*, Vol. 5, 1979, pp. 690–697.

[15]Fanson, J. L., and Chen, J. C., "Structural Control by the Use of Piezoelectric Active Members," *Proceedings of 1st NASA/DOD CSI Technology Conference* (Norfolk, VA), 1986, pp. 809–829.

[16]Fanson, J. L., Blackwood, G. H., and Chu, C. C., "Active Member Control of Precision Structures," *Proceedings of 30th AIAA Structures, Structural Dynamics, and Materials Conference* (Mobile, AL), AIAA, Washington, DC, 1989, pp. 1480–1494, AIAA Paper 89-1329.

[17]Fanson, J. L., Chu, C. C., Lurie, B. J., and Smith, R. S., "Damping and Structural Control of the JPL Phase 0 Testbed Structure," *Journal of Intelligent Material Systems and Structures*, Vol. 2, 1991, pp. 281–300.

[18]Preumont, A., Dufour, J. P., and Malekian, C., "Active Damping by a Local Force Feedback with Piezoelectric Actuators," *Journal of Guidance, Control, and Dynamics*, Vol. 15, 1992, pp. 390–395.

[19]Spangler, R. L., Jr., and Hall, S. R., "Robust Broadband Control of Flexible Structures Using Integral Piezoelectric Elements," 3rd International Conf. on Adaptive Structures [Paper], San Diego, CA, Nov. 1992, pp. 665–679.

[20]Spangler, R. L., Jr., and Hall, S. R., "Broadband Active Structural Damping Using Real Compensation and Piezoelectric Simultaneous Sensing and Actuation," *Smart Materials and Structures*, Vol. 3, 1994, pp. 448–458.

[21]Hagood, N. W., Chung, W. H., and Von Flotow, A., "Modelling of Piezoelectric Actuator Dynamics for Active Structural Control," *Proceedings of the AIAA/ASME/ASCE/AHS/ASC 31st Structures, Structural Dynamics, and Materials Conference* (Long Beach, CA), AIAA, Washington, DC, 1990, pp. 2242–2256.

[22]Cole, D. G., and Clark, R. L., "Adaptive Compensation of Piezoelectric Sensoriactuators," *Journal of Intelligent Material Systems and Structures*, Vol. 5, Sept. 1994, pp. 665–672.

[23]Cole, D. G., and Robertshaw, H. H., "Direct Rate Feedback for Piezostructures using Sensoriactuators with Feed Through Dynamics," *Proceedings of the Adaptive Structures Forum*, 1994.

[24]Hagood, N. W., and Anderson, E. H., "Simultaneous Sensing and Actuation Using Piezoelectric Materials," *Active and Adaptive Optical Components*, Vol. 1543, International Society for Optical Engineering, San Diego, CA, 1992, pp. 409–421.

[25]Widrow, B., and Stearns, S. D., *Adaptive Signal Processing*, Prentice–Hall, Englewood Cliffs, NJ, 1985.

[26]Balas, M. J., "Direct Velocity Feedback Control of Large Space Structures," *Journal of Guidance, Control, and Dynamics*, Vol. 2, No. 3, 1979, pp. 252, 253.

[27]Oppenheim, A. V., and Schafer, R. W., *Discrete-Time Signal Processing*, Prentice–Hall, Englewood Cliffs, NJ, 1989, Chap. 3.

[28]Vipperman, J. S., and Clark, R. L., "Hybrid Analog and Digital Adaptive Compensation of Piezoelectric Sensoriactuators," *Proceedings of the AIAA/ASME/ASCE/AHS/ASC 36th Structures, Structural Dynamics, and Materials Conference and AIAA/ASME Adaptive Structures Forum* (New Orleans, LA), AIAA, Washington, DC, 1995, pp. 2854–2859.